

Enhanced dynamics of active Brownian particle in a periodic array of obstacles and corrugated channel

Sudipta Pattanayak,^{1,*} Rakesh Das,^{1,†} Manoranjan Kumar,^{1,‡} and Shradha Mishra^{2,§}

¹*S. N. Bose National Centre for Basic Sciences,
J D Block, Sector III, Salt Lake City, Kolkata 700106*

²*Department of Physics, Indian Institute of Technology (BHU), Varanasi, India 221005*

Biological microorganisms and intercellular particles often encounter crowded environment during their motion. Here we study the motion of an active Brownian particle using overdamped Langevin dynamics on a two-dimensional substrate with periodic array of obstacles, and in a quasi-one-dimensional corrugated channel comprised of periodically arranged circular or elliptical obstacles at the boundary of the channel. The periodicity of the obstacles on the two-dimensional substrate enhances the persistence motion of the particle. Furthermore, we note ballistic transport of the particle in the corrugated channel without any external drive and the transport property is independent of the nature of the comprising obstacles. It depends on activity of the particle, width and periodicity of the channel. However, the particle does not show any ballistic transport in flat channel.

I. INTRODUCTION

Motion of self-propelled particles (SPPs) in two or three dimensional (2D or 3D) geometries has been an area of intense research in the last one decade [1–3]. SPPs in random [4] or regular arrays of rigid obstacles [5, 6], and also in the corrugated geometry [7] show many interesting phenomena. Some typical examples are the intercellular transport of cargoes by molecular motors, the motion of biological microswimmers and the motion of different active Janus particles [1–3, 8, 9]. Recently many experiments have been performed on biological microswimmers like swimming bacteria and motile cells, and artificial microswimmers like self-propelled emulsion droplets.

In a recent study [4], Stark *et al.* find that in 2D the presence of random obstacles leads a transition from diffusive to subdiffusive behaviour of an active Brownian particle (ABP) as the density of the obstacles approaches the percolation threshold. However, other studies [5, 6, 10, 11] show an enhanced ballistic transport of the SPPs in 2D periodic obstacle environment. The motion of the active Janus particle gets enhanced in the presence of random polymers [12]. Udit *et al.* have considered a collection of chemically boosted SPPs moving atop a 2D crystalline surface [6], and showed a change in the long-time diffusion constant depending on the relative strength of the activity and the trapping potential. Therefore, in the presence of the obstacles, the dynamics of the active particles can be *suppressed* or *enhanced* depending on their arrangement.

In this paper we study the dynamics of the ABP on a 2D substrate with periodically arranged obstacles. The ABP shows a crossover from its initial superdiffusive to

diffusive dynamics, and such a crossover is an intrinsic feature of the active particles [13–15]. But periodic array of obstacles introduce an enhanced dynamics, and the ABP performs more directed motion in comparison to its motion in the free space.

In the later part of this paper, the dynamics of the ABP in a confined geometry is studied. In the previous studies like transport of cargo in a corrugated channel [16], boundary controlled flow-induced phase separation of active particle [17] and boundary induced convection in a collection of polar SPPs [18], the effect of confinement on the dynamics of the active particles have been studied. The characteristics of the active particles in the presence of boundary are different from their equilibrium (passive) counterparts, as the active particles show anomalous diffusion [19, 20] in the confined geometries. Recently many experimental [21, 22] and theoretical [23–26] studies have described the motion of the SPPs under asymmetric potential. Angelani *et al.* [23] show that the run-and-tumble particles show a net drift speed under a periodic and asymmetric potential. Wan *et al.* [24] study the rectification phenomenon of overdamped swimming bacteria in an array of asymmetric barriers. A ballistic transport of active Janus particles is shown in periodically compartmentalized channel [25]. Potosky *et al.* [26] show that even under a symmetric potential a spatially modulated self-propelled velocity can induce directed transport.

In all of the above mentioned studies either the potential is asymmetric or the velocity of the active particles is spatially modulated. But there is no such study about the dynamics of the ABP in a periodic symmetric corrugated channel. Motivated by enhanced persistent motion of the ABP in a periodic 2D substrate, we have studied dynamics of the ABP in a quasi one-dimensional symmetric corrugated channel. We note that such corrugated channel governs a ballistic transport of the ABP along the channel without any external drive. Therefore, the dynamics of the ABP depends only on its activity and nature of the environment. This phenomenon is dif-

* sudipta.pattanayak@bose.res.in

† rakesh.das@bose.res.in

‡ manoranjan.kumar@bose.res.in

§ smishra.phy@itbhu.ac.in

ferent from the previous results, where the transport of the ABP is observed in the presence of asymmetric potential. Such boundary induced ballistic motion can help us to understand the transport phenomena in many biological systems.

Rest of this article is organised as follows. In section II we introduce the microscopic rule based model for the ABP in periodic geometries. The results of the numerical simulation of periodic 2D substrate and corrugated geometries are given in section III A and III B, respectively. Finally in section IV, we discuss our results and future prospect of our study.

II. MODEL

We consider a circular-disk shaped active Brownian particle of radius R_p placed in a periodic obstacle environment. Its dynamics is studied for two models; (i) in model I, we consider a 2D $L \times L$ square lattice, where circular-disk shaped obstacles of radius R_o are placed periodically at the vertices, and (ii) in model II, we consider a quasi-one-dimensional corrugated channel comprised of periodically arranged circular or elliptical obstacles at the boundary of the channel. The semi-major and the semi-minor axes of the elliptical obstacles are designated by $max(a', b')$ and $min(a', b')$, respectively. a' and b' are always chosen along the x and y -axes, respectively. For corrugated channel with circular obstacles $a' = b'$. The ABP moves along $\mathbf{e}(t)$ with self-propulsion speed v_0 , where $\mathbf{e}(t)$ represents the unit vector along the orientation of the ABP at time t . The dynamics of the ABP is governed by overdamped Langevin equation,

$$\frac{d\mathbf{r}(t)}{dt} = v_0\mathbf{e}(t) + \mu \sum_i \mathbf{F}_0^i, \quad (1)$$

$$\frac{d\mathbf{e}(t)}{dt} = \sqrt{2D^R}\boldsymbol{\eta}^R(t) \times \mathbf{e}(t), \quad (2)$$

where $\mathbf{r}(t)$ represents position vector of the ABP at time t . The first term on the right-hand-side (RHS) of Eq. 1 is due to the activity of the ABP. The second term represents steric force acting on the ABP due to its neighbouring obstacles, and it depends on the centre to centre separation r of the ABP from a neighbouring obstacle. We consider $\mathbf{F}_0 = -\nabla V$, where the steric interaction is incorporated by a *Weeks-Chandler-Anderson* potential.

$$V = 4\epsilon \left[\left(\frac{\sigma}{r}\right)^{12} - \left(\frac{\sigma}{r}\right)^6 \right] + \epsilon, \quad \text{for } r < r_{eff}, \\ = 0, \quad \text{for } r \geq r_{eff}. \quad (3)$$

Strength of the steric force is tuned by a parameter μ , which is 0 for the obstacle-free substrate and 1 for all other cases. We consider $\epsilon = 1.0$. In this study, we consider the ABP as a point particle and the effective radius of the obstacles for model I is $r_{eff} = R_p + R_o$. In model II, if \mathbf{r}_o be the position vector of the centre of an obstacle and θ is the angle of the relative distance

$\mathbf{r} - \mathbf{r}_o$ with respect to the x -axis, then $r_{eff} = R_p + a'b'/\sqrt{a'^2 \sin^2 \theta + b'^2 \cos^2 \theta}$. Here, $\sigma = r_{eff}/(2^{1/6})$. The rate of change of the orientation $\mathbf{e}(t)$ of the ABP is given by Eq. 2. D^R represents the rotational diffusion constant, and $\boldsymbol{\eta}^R = \eta_z^R \mathbf{e}_z$ is the stochastic torque with zero mean and Gaussian white noise correlations, *i.e.*,

$$\langle \boldsymbol{\eta}^R(t) \rangle = 0, \quad (4)$$

$$\langle \boldsymbol{\eta}^R(t_1) \otimes \boldsymbol{\eta}^R(t_2) \rangle = \delta(t_1 - t_2). \quad (5)$$

Note that the stochastic torque always point out of the substrate, *i.e.*, along the z -axis.

The schematic of the model I and II are shown in Fig. 1(a) and (b), respectively. Colors in Fig. 1 shows the intensity plot of the potential. White regions are zero-potential region, and repulsive potential increases from white to dark red. Fig. 1(a) depicts a square lattice with spacing $a = 1$. Circular-disk shaped obstacles with effective radius $r_{eff} = R_p + R_o = 0.49$ are placed at the vertices. The separation between surfaces of two neighbouring obstacles is given by $\delta = a - 2r_{eff}$, and the ABP can pass through the zero-potential space between the obstacles if $\delta > 0$. In Fig. 1(b) a corrugated channel of width d (*i.e.*, centre to centre separation of two neighbouring obstacles in the y -direction) is shown schematically. The channel is composed of elliptical or circular-disk shaped obstacles arrayed along the x -direction with periodicity a . The surface to surface separation between two neighbouring obstacles are $\delta = a - 2r_{eff}$ and $d_{min} = d - 2r_{eff}$ along the x and y -direction, respectively. We choose $\delta < 0$ and $d_{min} > 0$ such that the ABP remains confined in the channel and can move along the x -direction.

The dimensionless angular Peclet number is defined as

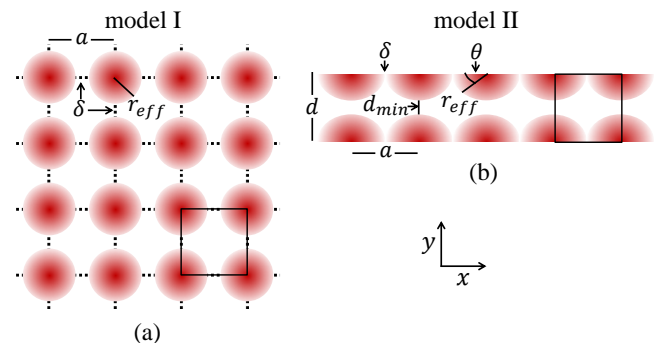


FIG. 1. (Color online) : (a) The schematic picture of a square lattice with obstacles at its vertices. Centre to centre distance between obstacles $a = 1.0$. The effective radius of the obstacles is $r_{eff} = 0.49$. The surface to surface separation of two neighbouring obstacles δ is shown here. (b) The schematic picture of a quasi-one-dimensional corrugated channel of circular / elliptical obstacles. The periodicity a , and width of the channel d are shown. r_{eff} (defined in the text) is shown. The surface to surface separation between two neighbouring obstacles along x and y directions are δ and d_{min} respectively. Boxes show unit cell for both cases. x and y directions for both model are shown.

$Pe = v_0/D_R R_p$. The persistent length of the particle is defined as $l = v_0/D_R$, and the corresponding persistent time $\tau = 1/D_R$. $D_R = 0.1$ is kept fixed, and the self-propulsion speed of the ABP v_0 is varied in our study. The closed boxes drawn in Fig. 1 (a) and (b) show the unit cells of the full periodic system. Initially the ABP with random velocity direction is placed randomly in one of the unit cells. The dynamics of the ABP is studied using the evolution Eqs. (1)-(2). Periodic boundary condition is used in both directions for model I and in x -direction (along the channel) for model II. Smallest time step $\Delta t = 10^{-3}$, and in some cases $\Delta t = 10^{-4}$. Simulation is done for total time steps 10^6 and 10^7 for model I and II, respectively. Averages are calculated over 10000 realisations.

III. RESULTS

A. Periodic substrate

We first study the dynamics of the ABP on a 2D substrate with periodic array of obstacles, *i.e.*, for model I. Typical trajectories of the ABP is shown in Fig. 2. The ballistic motion at the beginning for four ABPs with different initial direction is shown in Fig. 2(a). Four different colors are used for four ABPs. The trajectories of the four ABPs near the obstacles during their persistent motion is shown in Fig. 2 (b). Force due to obstacles make the dynamics slower and the ABP follows the obstacle boundary for some time. Colors have same meaning as in Fig. 2(a). Boxes in Fig. 2(a) and (b) show the end and the starting point of the trajectories, respectively. The late time trajectories of the ABP on the 2D substrate with periodic obstacles and in free space are shown in Fig. 2(c) and (d), respectively. Time difference between starting and end point of the trajectories $T (= 10^5 \Delta t)$ is same for Fig. 2(c) and (d). Interesting point to note from these two figures is that late time trajectory of the ABP shows more directional motion in a periodic environment in comparison to the free space.

To further characterize the motion of the ABP we calculate its mean square displacement (MSD) defined as

$$\langle \Delta r^2(t) \rangle = \frac{1}{N} \sum_{n=1}^N \left[(x_n(t) - x_n(0))^2 + (y_n(t) - y_n(0))^2 \right], \quad (6)$$

where N is the total number of ensembles, $x_n(t)$ and $y_n(t)$ represent position of the ABP at time t for the n^{th} ensemble in the $x-y$ plane. The MSD of the ABP in a periodic obstacle environment and in a free substrate for different Pe are shown in Fig. 3(a) and (b), respectively. The ABP performs persistent random walk (PRW), which is one of the common features in the active systems [4, 6, 10, 13]. Therefore, the MSD can be written as,

$$\langle \Delta r^2 \rangle = 2\mathcal{D}D_{eff}t \left[1 - \exp\left(-\frac{t}{t_c}\right) \right], \quad (7)$$

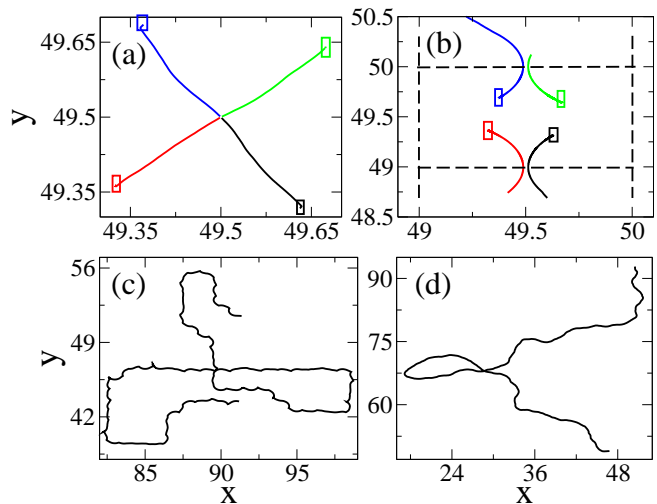


FIG. 2. (Color online) (a) Plot of ballistic trajectory at the beginning of four ABPs. Initial coordinate for all ABPs is $(49.5, 49.5)$, and their directions are different. Four different colors used for four ABPs. (b) Plot of the trajectory of the ABPs when they follow the obstacle boundary. The intersection points of the dotted lines represent centre of an obstacle. Same color in (a) and (b) represents same particle. The boxes in (a) represent the end point of the trajectories, and boxes in (b) represent the starting of the trajectories. Plot of late time diffusive trajectory of an ABP on a two dimensional substrate with and without obstacles are shown in (c) and (d) respectively. The time interval $T = 100(9 \times 10^5 \Delta t - 10^6 \Delta t)$. $Pe = 50$, and the effective radius of the obstacles $r_{eff} = 0.49$.

where \mathcal{D} represents dimensionality of the space, D_{eff} is the effective diffusion constant in the steady state, and t_c is the crossover time from initial ballistic regime $\langle \Delta r^2 \rangle = 4D_{eff}t^2/t_c$ for $t \ll t_c$ to late time diffusive regime $\langle \Delta r^2 \rangle = 4D_{eff}t$ for $t \gg t_c$. The two lines of slope 2 and 1 shown in Fig. 3 represent the ballistic (I) and the diffusive (III) regimes of the ABP, respectively, for different Pe . The crossover time t_c and diffusion constant D_{eff} are estimated by fitting the numerical data with Eq. (7). The crossover time t_c for the free environment does not change with Pe , but t_c changes with Pe for the periodic obstacle environment. The approximate change in t_c is shown by arrows in Fig. 3 (a) and (b). The ABP also realizes a small confinement effect (regime with label II) in the presence of the obstacles during its persistent motion, and MSD shows plateau for that time duration, which is shown in the inset of Fig. 3(a). The scaled MSD $\langle \Delta r^2 \rangle / 4D_{eff}t_c$ versus scaled time t/t_c for different Pe for the periodic obstacle and the free environment are plotted in Fig. 4(a) and (b), respectively. In both the cases data shows good scaling collapse. The plot of t_c versus Pe for the periodic obstacle (squares) and free substrate (circles) are shown in Fig. 4(c). The t_c changes with Pe for periodic obstacle substrate, whereas it is constant for free substrate. Also the t_c is larger for the periodic obstacle environment as compared to the free case. Therefore the periodicity enhances the persistence

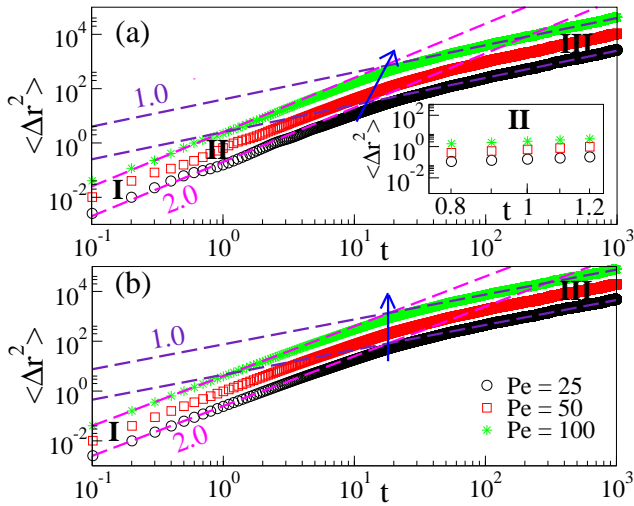


FIG. 3. (Color online) Plot of the mean square displacement of the ABP $\langle \Delta r^2 \rangle$ vs. time t in a periodic square lattice (a) with and (b) without obstacles. Region I and III are ballistic and diffusive regions of the ABP respectively. Line of slope 2 (magenta) and 1 (indigo) are shown. The approximate crossover point for superdiffusive to diffusive dynamics for different Pe for both cases are shown by a blue arrow. In inset of (a), $\langle \Delta r^2 \rangle$ with time for different Pe in region II (when ABP moves along obstacle boundary) is shown. r_{eff} is same as in Fig. 2.

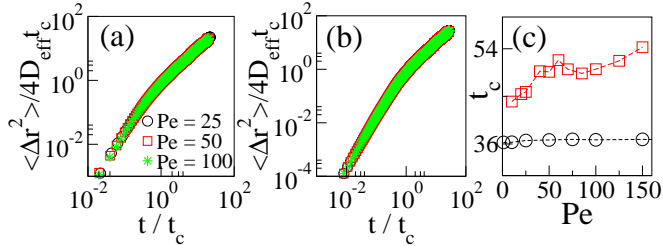


FIG. 4. (Color online) Plot of scaled mean square displacement $\langle \Delta r^2 \rangle / 4D_{eff}t_c$ vs. scaled time t/t_c of the ABP in the square lattice (a) with and (b) without obstacles are shown. (c) The crossover time t_c with Pe in a obstacle free (circles) and in a periodic obstacles substrate (squares) are shown. r_{eff} is same as in Fig. 2.

motion of the ABP.

Variation in the effective diffusion constant D_{eff} with Pe^2 for the periodic obstacle and free substrate are shown in Fig. 5(a). For the periodic obstacle and free substrate $D_{eff} \sim Pe^2$ with slope 0.0009 and 0.0018 respectively, which confirms the enhanced diffusion constant in the active systems, as found before in [27]. Interestingly, D_{eff} in the periodic (p) environment is exactly half of its value in the free (f) space. In the steady state, the MSD of the ABP can be expressed by $2\mathcal{D}_{eff}D_{eff}^{p/f}t$, where \mathcal{D}_{eff} is the effective dimensionality of the space and $D_{eff}^{p/f}$ represents the effective diffusivity in the periodic / free environment. Since $D_{eff}^p = \frac{1}{2}D_{eff}^f$, that implies the effective dimen-

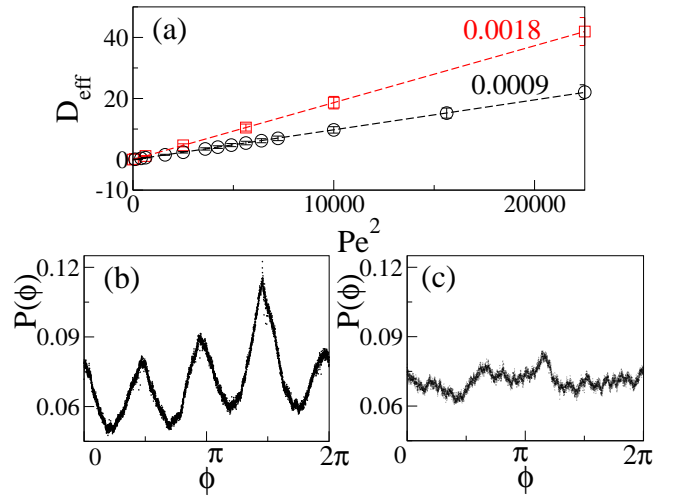


FIG. 5. (Color online) (a) Plot of the effective translational diffusion constant D_{eff} of the ABP for different Pe . The black circles and red squares are for the periodic obstacle environment and the free substrate respectively. (b-c) Plot of $P(\phi)$ of the ABP for periodic obstacles and free environment respectively. For (b) and (c) $Pe = 50$, and r_{eff} is same as in Fig. 2.

sionality for the system with periodic obstacles reduces to one. To further explain this, we calculate probability distribution function $P(\phi)$ of the instantaneous orientation ϕ of the ABP in the steady state. Plot of $P(\phi)$ for the periodic obstacle and the free substrate are shown in Fig. 5(b) and (c), respectively. $P(\phi)$ is flat for the free substrate, whereas it shows peaks in the periodic obstacle environment and magnitude of one peak is always larger. Therefore the ABP moving in a periodic obstacle environment shows directional preference during its motion. It explains why the D_{eff} of the ABP in periodic environment is half of its value in free space.

The periodic arrangement of the obstacles enhances the persistent motion of the ABP, and at the late time, the motion is more like one-dimensional persistent random walk. This phenomenon of the ABP is not present either in random obstacles [4] or in free environment. The immediate question arises what will happen if we restrict the motion of the ABP along one direction only. In the next part of this paper we study the dynamics of the ABP in a quasi-one-dimensional corrugated channel as shown in Fig. 1(b).

B. Corrugated channel

First we consider a corrugated channel comprised of circular-disk shaped obstacles with periodicity a and width d . The radii of each obstacle and the ABP are chosen as $R_o = 0.29$ and $R_p = 0.2$, respectively. The dynamics of the ABP is characterized by the MSD as defined in Eq. (6) and a MSD exponent β such that $\langle \Delta r^2(t) \rangle \sim t^\beta$.

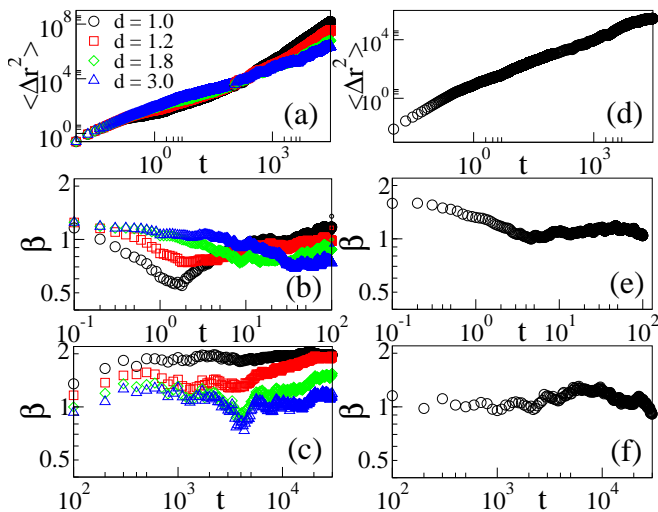


FIG. 6. (Color online) (a-c) Plot of the mean square displacement $\langle \Delta r^2 \rangle$, the exponent β in early and late time of the ABP in a corrugated channel for $Pe = 100$. (d-f) $\langle \Delta r^2 \rangle$, the exponent β in early and late time of the ABP in a flat repulsive channel of width $d = 0.42$ are shown respectively. For (a-c) $r_{eff} = 0.49$, for (d-f) $R_p = 0.2$ and $Pe = 50$.

This exponent β can also be defined as

$$\beta(t) = \log_{10} \frac{\langle \Delta r^2(10t) \rangle}{\langle \Delta r^2(t) \rangle}. \quad (8)$$

The exponent $\beta = 2$ and 1 for the ballistic and the diffusive dynamics, respectively. We show the MSD for a fixed $a = 0.75$ and different d in Fig. 6(a), and calculate β from these data. We note that at early time $t \lesssim 100$, the exponent $\beta < 1$, *i.e.*, the ABP exhibits subdiffusive dynamics for all d , as shown in Fig. 6(b). However, at the late time $t \gtrsim 100$, the ABP shows superdiffusive behavior ($\beta > 1$) only for narrow channels ($d = 1, 1.2$), whereas for wide channels ($d = 1.8, 3$), the dynamics is diffusive ($\beta = 1$). We note similar behavior for $Pe = 50$.

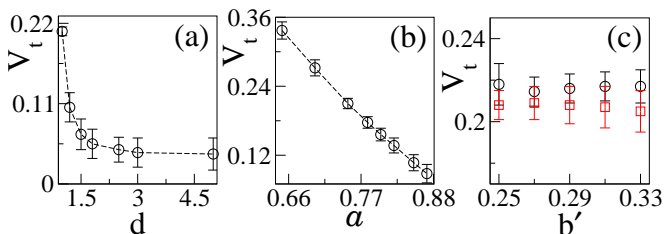


FIG. 7. (Color online) Plot of the transport speed V_t of the ABP with (a) the width d , and (b) the periodicity a of the corrugated channel of circular obstacles. $a = 0.75$ for (a), and $d_{min} = 0.02$ for (b). For all cases $Pe = 100$. (c) Plot of V_t of the ABP in a corrugated channel comprised of elliptical obstacles vs. b' . Two different $d_{min} = 0.005$ (circles), 0.02 (squares) are considered and $a' = 0.29$. Periodicity of the obstacles is $a = 0.75$, and $Pe = 100$. Error bar of V_t is shown for all cases.

To understand the importance of the corrugated geometry, we also calculate the MSD of the ABP in a quasi-one-dimensional channel with flat boundary. We note that the ABP performs diffusive motion in the flat geometry, as is evident from Fig. 6(d-f) drawn for channel width $d = 0.42$ and ABP radius $R_p = 0.2$. Therefore, the quasi-one-dimensional corrugated channel drives the ABP towards ballistic dynamics ($\beta \simeq 2$) at the late time, *i.e.*, induces directionality in the motion.

The induced directionality in the narrow corrugated channel motivates us to look for a net transport of the ABP through the channel. The transport is explored through statistical averages, specifically through the absolute value of the mean displacement, The transport speed is defined as $V_t = \sqrt{\langle \Delta r^2(t) \rangle} / v_0 t$. The V_t for different width d and periodicity a of the channel are shown in Fig. 7(a) and (b), respectively. We note that V_t decreases with increasing width d or increasing periodicity a . Therefore, narrow corrugated channels with closely placed circular-disk shaped obstacles speeds up the net transport of the ABP.

To study how the ballistic transport of the ABP depends on the nature of the comprising obstacles of the corrugated channel, we consider a quasi-one-dimensional symmetric corrugated channel comprised of elliptical-disk shaped obstacles, as described in Sec. II. The earlier described case of circular-disk shaped obstacles is a special case of the elliptical obstacles when $a' = b'$. We keep $a' = 0.29$ fixed, and vary b' to study the elliptical case. b' has been varied by varying the width d of the channel, such that d_{min} is kept fixed to a certain value. The variation in the transport speed V_t with b' is shown for different $d_{min} = 0.005, 0.02$ in Fig. 7(c). We note that V_t does not depend on b' , though it is higher for small d_{min} .

To further explain the ballistic transport of the ABP in a corrugated channel in detail we show the potential variation in a unit cell of the channel in Fig. 8. The potential variation in a unit cell for two different periodicity of the obstacles $a = 0.65, 0.75$ are shown in Fig. 8(a) and (b), respectively. The color bar shows the strength of the

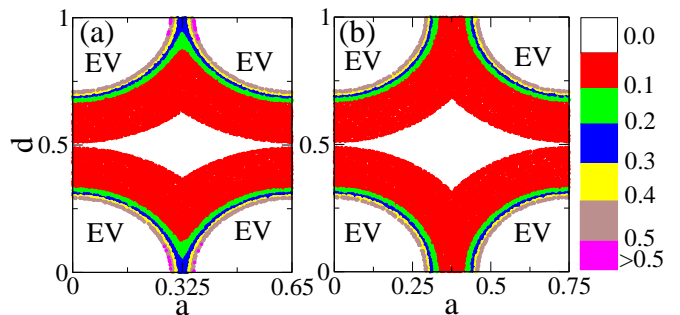


FIG. 8. (Color online) Plot of the potential variation inside a unit cell of the corrugated channel of circular obstacles for $a = 0.65$ and 0.75 are shown in (a) and (b) respectively. The color bar indicates the strength of the potential at different points. The effective radius of the obstacles is $r_{eff} = 0.49$.

potential at different point, and corners of the cells are not accessible to the ABP because of strong repulsive potential. Remember for $a = 0.65$ and 0.75 we get ballistic transport of the ABP along the channel. The ABP feels more repulsive force in the grooves for $a = 0.65$ compare to $a = 0.75$. For small a the ABP feels more repulsive force at the grooves and it does not stuck at the grooves. But for larger a the ABP feels less repulsive force at the grooves and it stays longer time there. Therefore the dynamics of the ABP is faster for small periodicity a of the corrugated channel.

IV. DISCUSSION

We have studied dynamics of an ABP in the presence of circular-disk shaped obstacles arrayed periodically on a 2D substrate. This periodic arrangement of the obstacles and the self-propulsion nature of the ABP lead to an enhanced persistent motion of the ABP, which is not present in the free [13] or in a random obstacle environment [4]. Our results are in good agreement with other studies of the active particles in a periodic obstacle environment [6, 10]. In the presence of the periodic obstacles, the crossover time from ballistic to diffusive dynamics of the ABP increases with activity. Therefore, the persistent length of the ABP increases in the periodic obstacle environment. The periodicity of obstacles also induces directionality in the dynamics of the ABP.

Motivated by the above mentioned phenomenon of the ABP, we have also studied the motion of the ABP in a quasi-one-dimensional corrugated channel, where mo-

tion of the ABP is confined along one direction. We find the ballistic transport of the ABP in the quasi-one-dimensional corrugated without any external drive. This makes our study different from the previous studies, where the net transport of the ABP is observed with some external force or spatially modulated velocity [21–26]. The transport of the ABP does not depend on the nature of the comprising obstacles (circular / elliptical) of the corrugated channel. It depends on the activity of the ABP, width and periodicity of the channel. However, the ABP does not show any ballistic transport in flat channel.

Hence the confinement, activity of the ABP and the periodicity of the channel lead to ballistic transport of the ABP without any external drive. Such transport useful to understand the dynamics of the active particles in many biological systems. This study helps us to design a device for efficient drug delivery. Experiment can be performed for our model to verify the dynamics of the ABP in periodic array of obstacle and confined corrugated channel. In our current study, we have ignored the inter-particle interaction. It is also interesting to study the dynamics of the interacting ABPs in different kinds of confined geometries.

V. ACKNOWLEDGEMENT

SP and SM would like to thank Department of Physics, Indian Institute of Technology (BHU), Varanasi and S. N. Bose National Centre for Basic Sciences respectively for their kind hospitality.

-
- [1] S. Ramaswamy, *Annu. Rev. Condens. Matter Phys.* **1**, 323 (2010).
 - [2] M. C. Marchetti, J. F. Joanny, S. Ramaswamy, T. B. Liverpool, J. Prost, Madan Rao and R. Aditi Simha, *Rev. Mod. Phys.* **85**, 1143 (2013).
 - [3] P. Romanczuk, M. Bär, W. Ebeling, B. Lindner and L. Schimansky-Geier, *Eur. Phys. J. Spec. Top.* **202**, 1 (2012).
 - [4] M. Zeitz, K. Wolff and H. Stark, *Eur. Phys. J. E* **40**, 23 (2017).
 - [5] F. Q. Potiguar, G. A. Farias and W. P. Ferreira, *Phys. Rev. E* **90**, 012307 (2014).
 - [6] U. Choudhury, A. V. Straube, P. Fischer, J. G. Gibbs and F. Höfling, *New J. Phys.* **19**, 125010 (2017).
 - [7] Bao-quan Ai, Qiu-yan Chen, Ya-feng He, Feng-guo Li and Wei-rong Zhong, *Phys. Rev. E* **88**, 062129 (2013).
 - [8] A. Zöttl and H. Stark, *J. Phys.: Condens. Matter* **28**, 253001 (2016).
 - [9] M. Polin, I. Tuval, K. Drescher, J. P. Gollub and R. E. Goldstein, *Science* **325**, 487 (2009).
 - [10] T. Chinnasamy, J. L. Kingsley, F. Inci, P. J. Turek, M. P. Rosen, B. Behr, E. Tüzel and U. Demirci, *Adv. Sci. (Weinh)* **5**, 1700531 (2018).
 - [11] J. P. Gleghorn, J. P. Smith and B. J. Kirby, *Phys. Rev. E* **88**, 032136 (2013).
 - [12] N. Samanta, R. Goswami and R. Chakrabarti, arXiv:1704.06207 [cond-mat.soft].
 - [13] Xiao-Lun Wu and A. Libchaber, *Phys. Rev. Lett.* **84**, 13 (2000).
 - [14] A. E. Patteson, A. Gopinath, P.K. Purohit and P.E. Arratia, *Soft Matter* **12**, 2365 (2016).
 - [15] K. Bisht, S. Klumpp, V. Banerjee and R. Marathe, *Phys. Rev. E* **96**, 052411 (2017).
 - [16] S. Dey, K. Ching and M. Das, *J. Chem. Phys.* **148**, 134907 (2018).
 - [17] S. Thutupalli, D. Geyer, R. Singh, R. Adhikari and H. A. Stone, *Proc. Natl. Acad. Sci.* **115**, 5403 (2018).
 - [18] S. Mishra, S. Pattanayak, *Physica A* **477**, 128 (2017).
 - [19] P. S. Burada, P. Hänggi, F. Marchesoni, G. Schmid and P. Talkner, *Chem. Phys. Chem.* **10**, 45 (2009).
 - [20] M. Mangeat, T. Guérin and D. S. Dean, *Europhys. Lett.* **118**, 4 (2017).
 - [21] R. Di Leonardo, L. Angelani, D. DellArciprete, G. Ruocco, V. Iebba, S. Schippa, M. P. Conte, F. Mecarini, F. De Angelis and E. Di Fabrizio, *Proc. Natl. Acad. Sci.* **107**, 9541 (2010); A. Sokolov, M. M. Apodaca, B. A. Grzybowski and I. S. Aranson, *Proc. Natl. Acad. Sci.*

- 107**, 969 (2010).
- [22] P. Galajda, J. Keymer, P. Chaikin and R. Austin, *J. Bacteriol.* **189**, 8704 (2007).
- [23] L. Angelani, A. Costanzo and R. Di Leonardo, *Europhys. Lett.* **96**, 68002 (2011); L. Angelani, R. Di Leonardo and G. Ruocco, *Phys. Rev. Lett.* **102**, 048104 (2009).
- [24] M. B. Wan, C. J. Olson Reichhardt, Z. Nussinov and C. Reichhardt, *Phys. Rev. Lett.* **101**, 018102 (2008).
- [25] P. K. Ghosh, V. R. Misko, F. Marchesoni and F. Nori, *Phys. Rev. Lett.* **110**, 268301 (2013).
- [26] A. Pototsky, A. M. Hahn and H. Stark, *Phys. Rev. E* **87**, 042124 (2013).
- [27] A. Baskaran and M. C. Marchetti, *Phys. Rev. Lett.* **101**, 268101 (2008).